A regime diagram for ocean geostrophic turbulence

Andreas Klocker,[1] David P. Marshall,[2] Shane R. Keating,[3] Peter L. Read[2]

[1]Institute for Marine and Antarctic Studies, University of Tasmania, Hobart, Tasmania, Australia

[2]Department of Physics, University of Oxford, Oxford, UK.

[3]School of Mathematics and Statistics, University of New South Wales, Sydney, New South Wales, Australia

A two-dimensional regime diagram for geostrophic turbulence in the ocean is constructed by plotting observation-based estimates of the nondimensional eddy radius and unsuppressed mixing length against a nonlinearity parameter equal to the ratio of the root-mean square eddy velocity and baroclinic Rossby phase speed. For weak nonlinearity, as found in the tropics, the mixing length mostly corresponds to the stability threshold for baroclinic instability whereas the eddy radius corresponds to the Rhines scale; it is suggested that this mismatch is indicative of the inverse energy cascade that occurs at low latitudes in the ocean and the zonal elongation of eddies. At larger values of nonlinearity, as found at mid- and high-latitudes, the eddy length scales are much shorter than the stability threshold, within a factor of 2.5 of the Rossby deformation radius. However, better agreement is found with a turbulent β length scale across much of the ocean.

1. Introduction

The ocean is a turbulent fluid with transient motions on a plethora of spatial and temporal scales. The large-scale circulation is dominated by the turbulent geostrophic eddy field, with an eddy spatial scale that correlates with the Rossby deformation radius [*Stammer*, 1997]. Interactions between the turbulent geostrophic eddies and the large-scale flow have a profound impact on the circulation and stratification of the global ocean [e.g., *Rhines and Young*, 1982; *Gent et al.*, 1995; *Wolfe and Cessi*, 2010; *Munday et al.*, 2013], yet will need to be parameterized in many numerical ocean models for the foreseeable future [e.g., *Fox-Kemper et al.*, 2013].

One common approach to eddy parameterization is to employ mixing length arguments to derive an eddy diffusivity proportional to an eddy velocity multiplied by an eddy length scale. This approach has been used to develop full eddy closures for both the atmosphere and the ocean (e.g., *Bretherton* [1966]; *Green* [1970]; *Stone* [1972]; *Held and Larichev* [1996]; *Visbeck et al.* [1997]; *Eden and Greatbach* [2008]; *Marshall and Adcroft* [2010]) but exactly what sets this eddy length scale remains an active topic of research.

The most comprehensive study of eddy length scales has been carried out by *Tulloch et al.* [2011] who found that observed eddy length scales exceed the energy injection scale at all latitudes, with the latter occurring at scales larger than the deformation radius at high latitudes, and at scales smaller than the deformation radius at low latitudes. Recently, *Klocker and Abernathey* [2014] have used two measures of the eddy length scale in order to estimate eddy diffusivities. The first is the eddy "radius" of *Chelton et al.* [2011]. The second is a mixing length scale inferred from a passive tracer field, modified

to remove the kinematic suppression of mixing by background mean flow [*Ferrari and Nikurashin*, 2010; *Klocker et al.*, 2012].

The aim of this short contribution is to introduce a *regime diagram* of geostrophic turbulence in the ocean in which these two observation-based estimates of eddy length scales correspond to different dynamical *regime transitions*. The manuscript is structured as follows. In section 2, we summarize the method of data analysis and describe the regime diagram. In section 3, we physically interpret the observation-based eddy length scales in terms of dynamical regime transitions. A brief concluding discussion is given in section 4.

2. The regime diagram

The regime diagram (Fig. 1) is constructed by plotting measures of a nonlinearity parameter, defined as the ratio of the root-mean squared eddy velocity and the Rossby phase speed [*Chelton et al.*, 2011], against eddy length scales, normalized by the baroclinic deformation radius. To calculate these variables we use nearly two decades worth of satellite measurements of sea-surface height (SSH). We focus on a region in the Pacific Ocean, ranging from 60^{o}S to 50^{o}N and 180^{o}W to 230^{o}W, which covers a wide parameter space of the regime diagram. The geostrophic flow is close to zonal in this region, enabling us to use zonal averages of flow properties.

The nonlinearity parameter, represented by the x-axis in the regime diagram, is defined following *Chelton et al.* [2011] as

$$r = \frac{U_{\mathrm{eddy}}}{c}, \tag{1}$$

where U_{eddy} is the root-mean squared eddy velocity, $c = \beta L_D^2$ is the long Rossby wave speed at which nonlinear eddies propagate westward [*Cushman-Roisin et al.*, 1990; *Chelton et al.*, 2007], β is the meridional gradient of the Coriolis parameter and L_D the deformation radius. Here U_{eddy} is calculated using SSH-derived geostrophic velocities. Since the calculation of the deformation radius requires knowledge of the stratification, we employ values for L_D from *Tulloch et al.* [2009] who used an ocean state estimate [*Forget*, 2010], i.e., an ocean model strongly constrained to observations, to calculate the Rossby wave speed in the long-wave limit. Note that these methods of estimating U_{eddy} and c are both different to those used by *Chelton et al.* [2007, 2011].

The normalized eddy length scales, represented by the y-axis in the regime diagram, can be written as L/L_D. Here L is either the observed eddy radius, $L = R_{obs}$, or the eddy mixing length, $L = L_{mix}$.

Eddy radii R_{obs} are calculated using an eddy tracking algorithm based on the same SSH field [*Chelton et al.*, 2011], with the eddy radius being defined as the radius of a circle of area equal to that enclosed by contours of SSH within the eddy around which the circum-average speed is maximum. R_{obs}/L_D is shown as red dots and crosses in Fig. 1, with dots representing the southern hemisphere and crosses representing the northern hemisphere.

Since the unsuppressed eddy tracer diffusivity is proportional to the eddy velocity multiplied by the eddy length scale, the meridional mixing length L_{mix} is derived by advecting a numerical tracer in the SSH-derived geostrophic velocity field and removing the sup-

pression effect [*Klocker and Abernathey*, 2014]. L_{mix}/L_D is shown as blue dots and crosses in Fig. 1.

To understand the geographical distribution of the nondimensional variables in the regime diagram we distinguish tropics, mid-latitudes and the Southern Ocean in the panels on the bottom of Fig. 1. We also plot the nonlinearity parameter (Eq. 1) versus latitude in Fig. 2. Small values (less than 1) are found in the tropics, with larger values (greater than 1) at mid- and high-latitudes; the maximum values are found in the Southern Ocean.

The data used in the regime diagram are the same as used in *Klocker and Abernathey* [2014]; more detail on their calculation can be found there. The only slight difference to *Klocker and Abernathey* [2014] is that we plot the normalized eddy radius as opposed to the normalized eddy diameter (their Fig. 5).

3. Regime transitions

We now come to the main purpose of this manuscript, which is to interpret the observation-based eddy length scales on the regime diagram in terms of pertinent regime transition lines. These regime transitions refer to boundaries along which there is change in dynamical behavior. This change may be abrupt, e.g., through the crossing of a stability threshold, or gradual, through the dominance of different physical processes to either side of the transition.

3.1. Transition from linear to nonlinear dynamics

Flow regimes can be categorized as predominantly linear or nonlinear depending on whether or not an eddy can be regarded as a linear wave disturbance propagating through

a nearly stationary flow. These regimes are distinguished using the *nonlinearity parameter* defined in Eq. (1) [*Chelton et al.*, 2011].

If $r > 1$, the rotational velocity of the eddy, U_{eddy}, exceeds its translational velocity, roughly approximated by the long Rossby wave speed, c [*Chelton et al.*, 2007]. Transforming coordinates into the co-moving frame results in closed streamlines within the eddy, i.e., an inner core that is able to advect tracers, and an outer ring that is capable of stirring tracers [*Early et al.*, 2011]. If $r \leq 1$, the translational velocity of the eddy exceeds its rotational velocity and transforming coordinates into the co-moving frame does not result in closed streamlines within the eddy. The latitude corresponding to $r = 1$ is termed the *critical latitude* [*Theiss*, 2004] and can be used to distinguish regions of isotropic turbulence ($r > 1$) from regions with anisotropic turbulence ($r < 1$) in which turbulence induces alternating zonal jets [*Okuno and Masuda*, 2003; *Theiss*, 2004].

In the regime diagram (Fig. 1) the change from linear to nonlinear dynamics is represented on the x-axis, with the line at the value of 1 (the magenta line in Fig. 1) being the regime transition line from linear dynamics (for values less than 1) to nonlinear dynamics (for values greater than 1).

The eddy length scales exhibit very different behavior to either side of the transition, with the two measures of eddy length departing from each other in the linear regime, but being broadly indistinguishable from each other in the nonlinear regime. In each of the linear and nonlinear regimes, a distinct functional variation of the eddy length scale with the nonlinearity parameter is obtained.

3.2. Transition from rotation- to stratification-dominated flow

Geophysical turbulence is strongly influenced by rotation and stable stratification with small Rossby number, $\mathrm{Ro} = U/fL$, and Froude number, $\mathrm{Fr} = U/c_{grav} = U/fL_D$, where U is a characteristic velocity scale, f is the Coriolis parameter, L is a characteristic eddy length scale and $c_{grav} = fL_D$ is the speed of an internal gravity wave. The relative importance of rotation and stratification is quantified by the *Burger number*,

$$Bu = \frac{\mathrm{Ro}^2}{\mathrm{Fr}^2} = \frac{L_D^2}{L^2}. \tag{2}$$

In a rotation-dominated flow, typical length scales are larger than the deformation radius, whereas in stratification-dominated flow, typical length scales are smaller than the deformation radius. In energetically favoured scales of motion in stably-stratified flow, the Burger number is O(1) leading to length scales of O(L_D) [*Read*, 2001].

In the regime diagram (Fig. 1) the influence of rotation and stratification is represented on the y-axis, with the line at the value of 1 (the green line in Fig. 1), i.e. length scales equal to the deformation radius, being the regime transition line between rotation-dominated flow (for values greater than 1) to stratification-dominated flow (for values less than 1).

Note that the eddy scale at which the transition occurs from linear to nonlinear dynamics coincides roughly with the transition from stratification- to rotation-dominated flow (more precisely this occurs at $L/L_D \approx 0.8$). In the nonlinear regime, the observed eddy length scales exceed the deformation radius by only a modest amount (typically a factor between 1 and 2, with values of 2.5 in the Southern Ocean); we also observe a much greater spread in both eddy length scales in the rotation-dominated regime ($L/L_D > 1$).

3.3. Transition from stable to unstable flow

Mesoscale eddies derive their energy primarily from baroclinic instability. Using the original argument for baroclinic adjustment [*Stone*, 1978], based on the condition for marginal criticality for baroclinic zonal flow in the two-layer quasigeostrophic (QG) model [*Phillips*, 1951], the *criticality parameter* can be written [*Held and Larichev*, 1996] as

$$\xi = \frac{\overline{U}_{\text{thermal}}}{c} = \frac{\overline{U}_{\text{thermal}}}{\beta L_D^2}, \tag{3}$$

where $\overline{U}_{\text{thermal}}$ is the mean zonal velocity from the thermal wind relation and $\xi > 1$ is the criterion or baroclinic instability in an inviscid flow. Equivalently, using the thermal wind relation, this criticality parameter can be expressed as a critical value of the meridional temperature gradient [*Stone*, 1978].

In supercritical mean states, $\xi > 1$, the flow is baroclinically unstable leading to turbulent flow in the form of mesoscale eddies, possibly with an inverse energy cascade from the scale of the instability towards the Rhines scale through nonlinear eddy-eddy interactions. These mesoscale eddies then enhance the meridional eddy flux of temperature, bringing the meridional temperature gradient towards its critical value – a process that has been termed *baroclinic adjustment* [*Stone*, 1978].

The criticality parameter ξ is closely related to the deformation radius, the Rhines scale and the nonlinearity parameter. To see this, we use the result from *Held and Larichev* [1996] that the root-mean squared eddy velocity is related to the mean thermal wind by

$$U_{\text{eddy}} \approx \frac{L}{L_D}\overline{U}_{\text{thermal}}, \tag{4}$$

derived by scaling the eddy potential vorticity flux and the implied eddy energy production, and assuming an inverse cascade. Thus the condition for baroclinic instability in

this limit can be rewritten

$$\frac{L}{L_D} \gtrsim r, \tag{5}$$

i.e., mesoscale eddies can only grow if their nondimensional length scale exceeds the nonlinearity parameter. In the following we use the term *stability threshold* to describe this transition between baroclinic unstable and stable flow, i.e., the state of marginal criticality.

In the regime diagram (Fig. 1) the stability threshold is shown as a black dashed line, with flow above this line being baroclinically stable and below this line being baroclinically unstable.

For $r < 1$ the unsuppressed eddy mixing length scale lies close to the stability threshold over much of the data points (with some smaller values in the northern hemisphere). However, for $r > 1$ the stability threshold lies within the rotation-dominated regime in which motion along the rotation axis, and hence release of available potential energy, is inhibited by rotational constraints; instead, the energy release occurs on scales comparable to the deformation radius consistent with baroclinic instability theory [*Charney*, 1948; *Eady*, 1949; *Phillips*, 1951]. *Tulloch et al.* [2011] calculated the most unstable length scales for the global ocean and finds that these slightly exceed the deformation radius at mid- and high latitudes, consistent with Fig. 1 for $r > 1$.

3.4. Transition from weak to strong Rossby elasticity

Just as stable stratification inhibits vertical motion, so the variation of the Coriolis parameter with latitude inhibits meridional motion. The Rossby restoring force arises through considering the vorticity dynamics acting on a line of fluid parcels and gives rise

to westward propagation. See a standard text such as *Vallis* [2006] for discussion of the Rossby wave mechanism and *Marshall and Pillar* [2011] for a physical interpretation of the Rossby restoring force.

The efficiency of the Rossby restoring force or *Rossby elasticity* [*Dritschel and McIntyre*, 2008] is quantified by considering the ratio of planetary vorticity variations and relative vorticity anomalies, with the transition occurring at the *Rhines scale*,

$$L_{\mathrm{Rhines}} = \sqrt{\frac{U_{\mathrm{eddy}}}{\beta}} \tag{6}$$

[*Rhines*, 1975]. In the regime diagram (Fig. 1) the transition from weak to strong Rossby elasticity is represented by the thick black line.

Below this transition, Rossby elasticity is insufficient to prevent turbulent mixing across latitude circles, whereas above this transition, strong Rossby elasticity prevents significant meridional displacements and Rossby waves dominate [although see *Sukoriansky et al.*, 2007, for a more careful discussion]. An alternative physical interpretation is that closed potential vorticity contours can occur on scales shorter than the Rhines scale, but not above.

For $r < 1$, we find that the two nondimensional eddy lengths diverge from each other, with the mixing length coinciding with the stability threshold, but the eddy radius coinciding with the Rhines scale. These results may be suggestive of an inverse energy cascade following the ideas of *Kraichnan* [1967], with energy cascading upscale from the energy injection scale at the stability threshold towards the Rhines scale at which Rossby waves can induce alternating zonal flows [*Rhines*, 1975; *Theiss*, 2004].

For $r > 1$, the observed eddy scales coincide with each other and are much shorter than the Rhines scale. The latter can be understood by rewriting the nonlinearity parameter, using Eq. (6), as

$$r = \left(\frac{L_{\mathrm{Rhines}}}{L_D}\right)^2 \tag{7}$$

and recalling that the observed eddy length scales are roughly equal to (a small multiple of) the deformation scale in this regime. Consistent with *Tulloch et al.* [2011], the observed eddy scales are very much smaller than the Rhines scale in this regime. *Tulloch et al.* [2011] identify a slight mismatch between the energy injection scale and observed eddy length scale which they identify with a limited inverse cascade.

3.5. Turbulent β scale

Finally, we discuss the relation of our results to the length scale formed from the turbulent energy flux or injection rate, ϵ, and the meridional gradient in the Coriolis parameter [*Vallis and Maltrud*, 1993],

$$L_\beta = \frac{\epsilon^{1/5}}{\beta^{3/5}}. \tag{8}$$

Vallis [2006] argues that this turbulent β scale is more fundamental than the Rhines scale to the extent that the energy flux is less likely to depend on β than the root-mean squared eddy velocity. Moreover *Sukoriansky et al.* [2007] have argued that the turbulent β scale and Rhines scale can differ and that the latter is a more accurate measure of the threshold of anisotropization of the inverse cascade through the transition from turbulent to Rossby wave dynamics. A key nondimensional parameter describing a transition in turbulent flows with a β effect is therefore the ratio of the Rhines scale to the turbulent β scale

[*Sukoriansky et al.*, 2007]

$$R_\beta = \frac{L_{Rhines}}{L_\beta}. \tag{9}$$

Using the present definitions of L_{Rhines} and L_β, the zonostrophic regime of *Galperin et al.* [2006] is characterized by $R_\beta \gtrsim \sqrt{2}$ and the frictional regime is characterized by $R_\beta \lesssim \sqrt{1.5}$. As suggested previously by *Sukoriansky et al.* [2007], the ocean is close to a transitional regime where $\sqrt{1.5} \lesssim R_\beta \lesssim \sqrt{2}$, which would point towards the inverse cascade in the ocean being arrested short of the Rhines scale.

To test this hypothesis, in Fig. 3, we plot an estimate of the nondimensional turbulent β scale on the same regime diagram as in Fig. 1. We first rewrite this ratio as

$$\frac{L_\beta}{L_D} = \frac{\epsilon^{1/5}}{\beta^{1/10}\, c^{1/2}} \tag{10}$$

where we have used that $c = \beta L_D^2$. The advantage of (10) is that the nondimensional turbulent β scale depends weakly on both ϵ and β: the variation in the latter is less than 7% between the equator and 60°, and the variation in the former due to an order of magnitude (factor of 10) uncertainty is by a factor of just 1.6. Thus the variation of L_β/L_D in (10) is dominated by the variation of the inverse square-root of the Rossby wave speed, c. In Fig. 3, we have taken $\epsilon = 4 \times 10^{-9}$, which is in the range of ϵ values estimated from satellite observations and high-resolution ocean models by [*Arbic et al.*, 2014, their Figs. 10 and 11], and chosen to give the best fit to the observation-based data.

We see in Fig. 3 that the theoretical prediction (10) captures much of the observed variation of the observed eddy length scale with latitude, in particular when the latter is identified as the unsuppressed mixing length. In the linear regime, $r < 1$, the ratio L_β/L_D is able to explain both the near-constant variation of L/L_D with r in the northern

hemisphere and the departures from this linear variation in the southern hemisphere. In the moderately nonlinear regime, $1 < r \lesssim 3.5$, the ratio L_β/L_D explains the systematic discrepancy between the Rhines scale and the observed eddy scale, with the latter being smaller by a factor not inconsistent with the transitional regime suggested by *Sukoriansky et al.* [2007]. At larger values of $r > 4$, the ratio L_β/L_D exceed the observed nondimensional eddy length scale, by a substantial amount at the very high values of r obtained in the Southern Ocean (not shown). Nevertheless there is sufficient qualitative similarity between the variation of L_β/L_D and L/L_D with r to suggest the two are closely related, notwithstanding that in reality ϵ is far from spatially uniform.

4. Concluding remarks

In this paper, we have introduced a two-dimensional regime diagram for geostrophic turbulence in the ocean. The axes correspond to the nonlinearity parameter and the eddy length scale, normalized by the deformation radius. Two observation-based measures of the eddy length scale are plotted on the diagram, corresponding to the eddy radius and the eddy mixing length (with suppression effects of the mean flow removed).

We have shown that the observed eddy length scales coincide roughly with different regime transitions on the diagram. In the linear regime, obtained in the tropics, the eddy radius corresponds to the Rhines scale whereas the eddy mixing length corresponds to the stability threshold. In the nonlinear regime, both the eddy radius and eddy mixing length correspond to (a small multiple of) the deformation radius. These results are consistent with previous studies, e.g., *Tulloch et al.* [2011] and references therein. However, good agreement is obtained between the observed eddy mixing scale and the turbulent β

scale across a wide range of parameter space, albeit without taking into account spatial variations in the turbulent energy flux.

One limitation of this study is that the role of mean flows has only been taken into account in the calculation of unsuppressed mixing lengths, but effects of the mean flow on the mean potential vorticity gradient, as shown to be important by *Theiss* [2006], and the advection of baroclinic eddies by depth mean flow [*Klocker and Marshall*, 2014], have been ignored. A further limitation is that we have been unable to fully distinguish between the barotropic and baroclinic components of the flow, for which the properties of the turbulent cascade differ [e.g., *Salmon*, 1998]. These issues should be addressed in future studies.

The eddy length scale is an important quantity for constructing parameterizations of geostrophic eddies. Specifically mixing length arguments are used to express the eddy diffusivity as proportional to an eddy velocity multiplied by an eddy length scale. The variation of the eddy radius on the regime diagram is broadly consistent with the simple proposal of *Eden and Greatbach* [2008] that the eddy length scale is given by the minimum of the Rhines scale and the deformation radius. However, as noted by *Fox-Kemper et al.* [2013], small differences between the observed eddy length scale and the deformation radius (up to 2.5 in the nonlinear regime) can make a large difference when it comes to practical implementation of a parameterization. A more accurate predictor of the unsuppressed eddy mixing length scale appears to be provided by the turbulent β length scale. This length scale also agrees with the conjecture that the diffusion coefficient of

the poleward heat transport depends on the turbulent energy flux ϵ [*Held and Larichev*, 1996; *Held*, 1999; *Lapeyre and Held*, 2003].

An interesting avenue for future research would be to plot the observed eddy radii and mixing lengths for flows in other rotating, stratified fluids such as the atmospheres of the Earth and giant gas planets, to determine whether the regimes we find in the ocean occur more widely. Work in this direction by *Cho and Polvani* [1996] has shown that using a simple shallow-water model and the observed values of radius, rotation rate, average wind velocity, and mean layer thickness, all of which are used in the calculation of the deformation radius and the Rhines scale, it is possible to reproduce observations of the flow on Jupiter, Saturn, Uranus and Neptune. Additionally, *Theiss* [2006] showed that when taking into account a finite deformation radius and a zonal mean flow, the nonlinearity parameter is very successful in distinguishing regions with alternating zonal flows and storms on Jupiter. These results therefore suggest that the regime diagram introduced here might be more universal.

Acknowledgments. The authors thank Ross Tulloch for providing data and Dudley Chelton, Boris Gaplerin and Michael McIntyre for useful discussions which helped to improve this manuscript. This work started during a visit of AK to the University of Oxford supported by an Australian Bicentennial Fellowship. AK was supported by a Australian Research Council Discovery Early Career Researcher Award. SRK was suppported by a UNSW Faculty Research Grant. DPM was partially supported by the Oxford Martin School.

References

306 Arbic, B. K., M. Müller, J. G. Richman, J. F. Shriver, A. J. Morton, R. B. Scott,
307 G. Sérazin, and T. Penduff (2014), Geostrophic turbulence in the frequency-wavenumber
308 domain: Eddy-driven low-frequency variability, *J. Phys. Oceanogr.*, *44*, 2025–2069.

309 Bretherton, F. P. (1966), Critical layer instability in baroclinic flows, *Quart. J. Roy.*
310 *Meteor. Soc.*, *92*, 325–334.

311 Charney, J. G. (1948), On the scale of atmospheric motions, *Geofys. Publ. Oslo*, *17*, 1–17.

312 Chelton, D. B., M. G. Schlax, R. M. Samelson, and R. A. de Szoeke (2007),
313 Global observations of large oceanic eddies, *Geophys. Res. Lett.*, *34*, L15,606,
314 doi:10.1029/2007GL030,812.

315 Chelton, D. B., M. G. Schlax, and R. M. Samelson (2011), Global observations of nonlinear
316 mesoscale eddies, *Prog. Oceanogr.*, *91*, 167–216.

317 Cho, J. Y.-K., and M. Polvani (1996), The morphogenesis of bands and zonal winds in
318 the atmosphere on the giant outer planets, *Science*, *273*, 335–337.

319 Cushman-Roisin, B., E. P. Chassignet, and B. Tang (1990), Westward motion of mesoscale
320 eddies, *J. Phys. Oceanogr.*, *20*, 758,768.

321 Dritschel, D. G., and M. E. McIntyre (2008), Multiple jets as PV staircases: The Phillips
322 effect and the resilience of eddy-transport barriers, *J. Atmos. Sci.*, *65*, 855–874.

323 Eady, E. T. (1949), Long waves and cyclone waves, *Tellus*, *1*, 33–52.

324 Early, J. J., R. M. Samelson, and D. B. Chelton (2011), The evolution and propagation
325 of quasigeostrophic ocean eddies., *J. Phys. Oceanogr.*, *41*, 1535–1555.

Eden, C., and R. J. Greatbach (2008), Towards a mesoscale eddy closure, *Ocean Modell.*, *20*, 223–239.

Ferrari, R., and M. Nikurashin (2010), Suppression of eddy diffusivity across jets in the Southern Ocean, *J. Phys. Oceanogr.*, *40*, 1501–1519.

Forget, G. (2010), Mapping ocean observations in a dynamical framework: A 2004-06 ocean atlas, *J. Phys. Oceanogr.*, *40*, 1201–1221.

Fox-Kemper, B., R. Lumpkin, and F. O. Bryan (2013), Ocean circulation and climate: A 21st century perspective, in *Lateral Transport in the Ocean Interior*, edited by G. Siedler, S. M. Griffies, J. Gould, and J. A. Church, pp. 185–209, Elsevier.

Galperin, B., S. Sukoriansky, N. Dikovskaya, P. L. Read, Y. H. Yamazaki, and R. Wordsworth (2006), Anisotropic turbulence and zonal jets in rotating flows with a β-effect, *Phys. Scr.*, *13*, 83–98.

Gent, P. R., J. Willebrand, T. J. McDougall, and J. C. McWilliams (1995), Parameterizing eddy-induced tracer transports in ocean circulation models, *J. Phys. Oceanogr.*, *25*, 463–474.

Green, J. S. A. (1970), Transfer properties of the large-scale eddies and the general circulation of the atmosphere, *Quart. J. Roy. Meteor. Soc.*, *96*, 157–185.

Held, I. M. (1999), The macroturbulence of the troposphere, *Tellus*, *51A*, 59–70.

Held, I. M., and V. D. Larichev (1996), A scaling theory for horizontally homogeneous, baroclinically unstable flow on a beta plane, *J. Atmos. Sci.*, *53*, 946–953.

Klocker, A., and R. Abernathey (2014), Global patterns of mesoscale eddy properties and diffusivities, *J. Phys. Oceanogr.*, *44*, 1030–1046.

348 Klocker, A., and D. P. Marshall (2014), Advection of baroclinic eddies by depth mean
349 flow, *Geophys. Res. Lett.*, *41*, 3517–3521.

350 Klocker, A., R. Ferrari, and J. H. LaCasce (2012), Estimating suppression of eddy mixing
351 by mean flows, *J. Phys. Oceanogr.*, *42*, 1566–1576.

352 Kraichnan, R. H. (1967), Inertial ranges in two-dimensional turbulence, *Phys. Fluids*, *10*,
353 1417–1423.

354 Lapeyre, G., and I. M. Held (2003), Diffusivity, kinetic energy dissipation, and closure
355 theories for the poleward eddy heat flux, *J. Atmos. Sci.*, *60*, 2907–2916.

356 Marshall, D. P., and A. J. Adcroft (2010), Parameterization of ocean eddies: Potential
357 vorticity mixing, energetics and Arnold's first stability theorem, *Ocean Modell.*, *32*,
358 188–204.

359 Marshall, D. P., and H. R. Pillar (2011), Momentum balance of the wind-driven and
360 meridional overturning circulation, *J. Phys. Oceanogr.*, *41*, 960–978.

361 Munday, D. R., H. L. Johnson, and D. P. Marshall (2013), Eddy saturation of equilibrated
362 circumpolar currents, *J. Phys. Oceanogr.*, *43*, 507–532.

363 Okuno, A., and A. Masuda (2003), Effect of horizontal divergence on the geostrophic
364 turbulence on a beta-plane: Suppression of the Rhines effect, *Phys. Fluids.*, *15*, 56–65.

365 Phillips, N. A. (1951), A simple three-dimensional model for the study of large-scale
366 extratropical flow patterns, *J. Meteor.*, *8*, 381–393.

367 Read, P. (2001), Transition to geostrophic turbulence in the laboratory, and as a paradigm
368 in atmospheres and oceans, *Survey Geophys.*, *22*, 265–317.

Rhines, P., and W. Young (1982), Homogenization of potential vorticity in planetary gyres, *J. Fluid Mech.*, *122*, 347–367.

Rhines, P. W. (1975), Waves and turbulence on a β-plane, *J. Fluid Mech.*, *69*, 417–443.

Salmon, R. (1998), *Lectures on Geophysical Fluid Dynamics*, Oxford University Press.

Stammer, D. (1997), Global characteristics of ocean variability estimated from regional TOPEX/POSEIDON altimeter measurements, *J. Phys. Oceanogr.*, *27*, 1743–1769.

Stone, P. H. (1972), A simplified radiative-dynamical model for the static stability of rotating atmospheres, *J. Atmos. Sci.*, *29*, 405–418.

Stone, P. H. (1978), Baroclinic adjustment, *J. Atmos. Sci.*, *35*, 561–571.

Sukoriansky, S., B. Galperin, and N. Dikovskaya (2007), On the arrest of inverse energy cascade and the Rhines scale, *J. Atmos. Sci.*, *64*, 3312–3327.

Theiss, J. (2004), Equatorward energy cascade, critical latitude, and the predominance of cyclonic vortices in geostrophic turbulence, *J. Phys. Oceanogr.*, *34*, 1663–1678.

Theiss, J. (2006), A generalized Rhines effect and storms on Jupiter, *Geophys. Res. Lett.*, *33*, doi:10.1029/2005GL025,379.

Tulloch, R., J. Marshall, and K. S. Smith (2009), Interpretation of the propagation of surface altimetric observations in terms of planetary waves and geostrophic turbulence, *J. Geophys. Res.*, *114*, C02,005, doi:10.1029/2008JC005,055.

Tulloch, R., J. Marshall, C. Hill, and K. S. Smith (2011), Scales, growth rates and spectral fluxes of baroclinic instability in the ocean, *J. Phys. Oceanogr.*, *41*, 1057–1076.

Vallis, G. K. (2006), *Atmospheric and Oceanic Fluid Dynamics*, 745 pp., Cambridge University Press.

Vallis, G. K., and M. E. Maltrud (1993), Generation of mean flows and jets on a beta plane over topography, *J. Phys. Oceanogr.*, *23*, 1346–1362.

Visbeck, M., J. Marshall, and T. Haine (1997), Specifcation of eddy transfer coefficients in coarse-resolution ocean circulation models, *J. Phys. Oceanogr.*, *27*, 381–403.

Wolfe, C. L., and P. Cessi (2010), What sets the strength of the middepth stratification and overturning circulation in eddying ocean models?, *J. Phys. Oceanogr.*, *40*, 1520–1538.

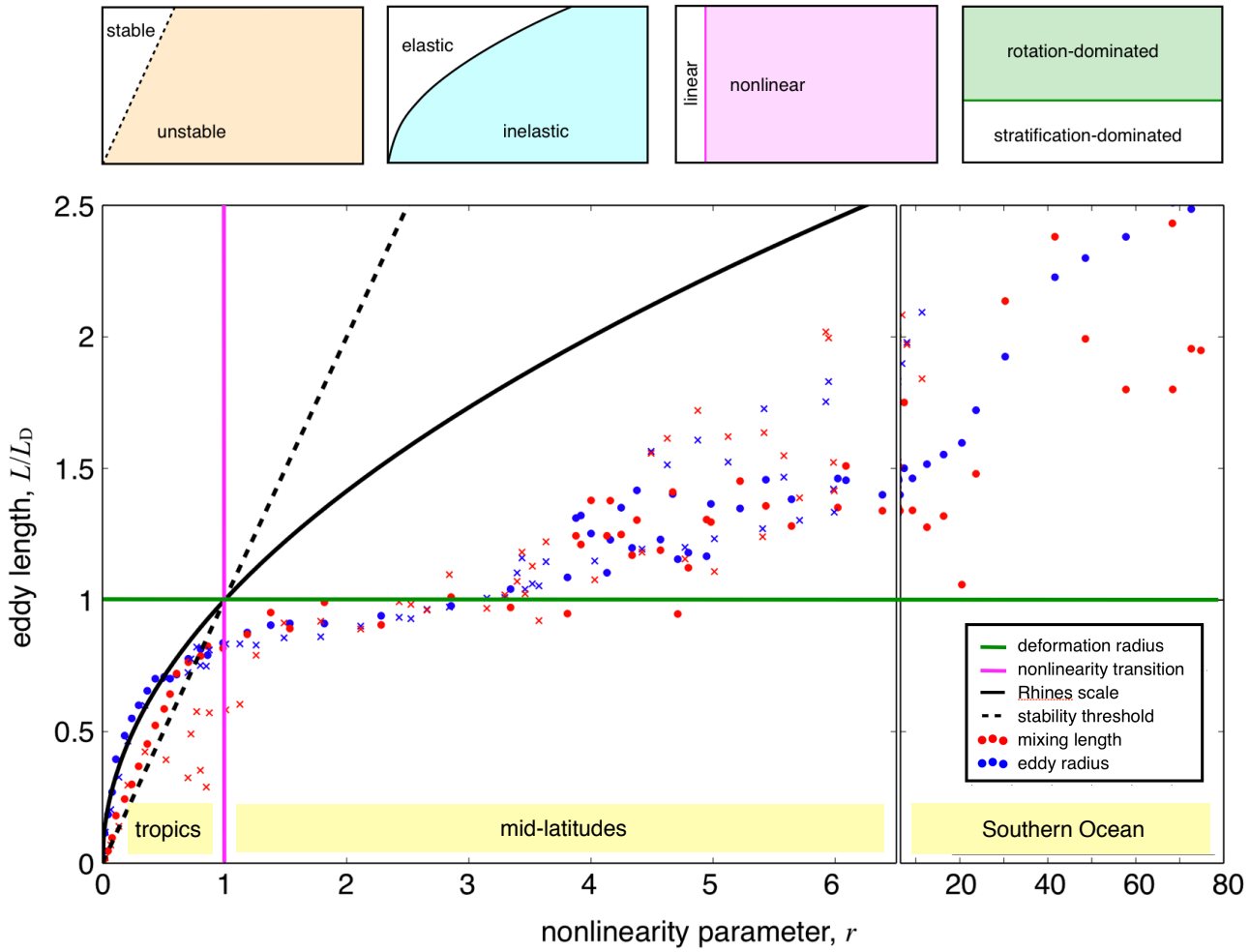

Figure 1. The regime diagram for ocean geostrophic turbulence. The axes correspond to the nonlinearity parameter, r, and the nondimensional eddy length scales, L/L_D. The blue symbols correspond to the nondimensional eddy radius and the red symbols to the nondimensional mixing length; dots are for the southern hemisphere and crosses for the northern hemisphere. The dashed black line is the stability threshold, the solid black line is the Rhines scale, the magenta line is the nonlinearity transition, and the green line is the deformation radius. These lines represent regime transitions from one dynamical regime to another as indicated in the upper panels. For further details, see the main text.

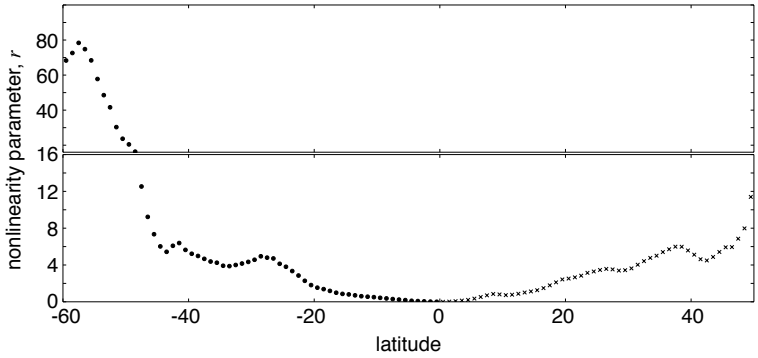

Figure 2. Variation of the nonlinearity parameter, r, with latitude. Dots correspond to the southern hemisphere and crosses to the northern hemisphere, as in Fig. 1.

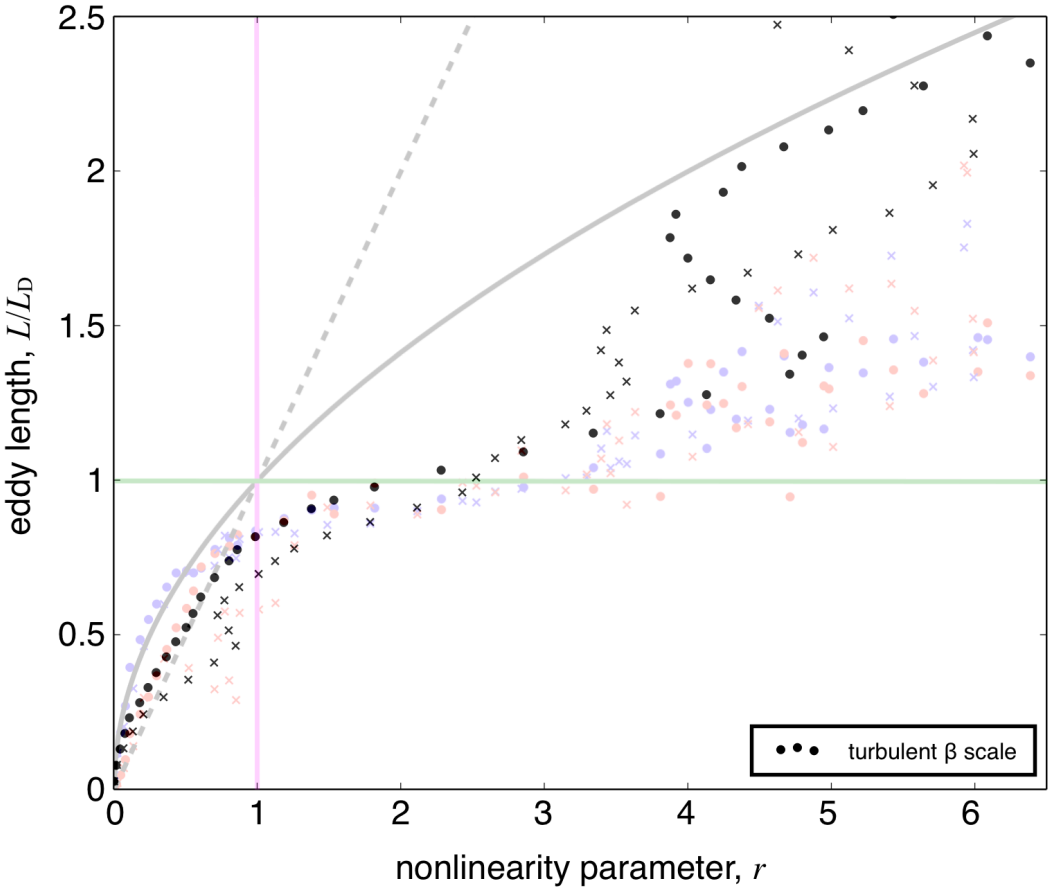

Figure 3. The nondimensional turbulent β scale, L_β/L_D, with $\epsilon = 4 \times 10^{-9}\,\mathrm{m^2 s^{-3}}$, plotted on the same regime diagram as in Fig. 1 for $r \leq 6.5$. Black dots are for the northern hemisphere and black crosses are for the southern hemisphere. The data and regime transitions lines from Fig. 1 are shown in faint in the background.